Longitudinal PET Monitoring of Amyloidosis and Microglial Activation in a Second Generation Amyloid-beta Mouse Model

Christian Sacher[1*], Tanja Blume[1,2*], Leonie Beyer[1*], Finn Peters[2], Florian Eckenweber[1], Carmelo Sgobio[2], Maximilian Deussing[1], Nathalie L. Albert[1], Marcus Unterrainer[1], Simon Lindner[1], Franz-Josef Gildehaus[1], Barbara von Ungern-Sternberg[1], Irena Brzak[3], Ulf Neumann[3], Takashi Saito[4], Takaomi C. Saido[4], Peter Bartenstein[1], Axel Rominger[1,5,6], Jochen Herms[2,5,7*], Matthias Brendel[1,5*]

[1]Dept. of Nuclear Medicine, University Hospital of Munich, LMU Munich, Munich Germany

[2]DZNE - German Center for Neurodegenerative Diseases, Munich, Germany

[3]Neuroscience, Novartis Institutes for BioMedical Research (NIBR), Basel, Switzerland

[4]Laboratory for Proteolytic Neuroscience, RIKEN Center for Brain Science, Saitama, Japan

[5]Munich Cluster for Systems Neurology (SyNergy), Munich, Germany

[6]Department of Nuclear Medicine, Inselspital, University Hospital Bern, Bern, Switzerland.

[7]Center of Neuropathology and Prion Research, University of Munich, Germany

*Contributed equally

11/05/2019

Short title: Micro-PET in *App*$^{NL-G-F}$ mice

Key words: Alzheimer's disease; β-amyloid; microglia; *App*$^{NL-G-F}$; spatial learning

Word count: 4996

Corresponding author:
Matthias Brendel MD; Department of Nuclear Medicine; LMU Munich, Germany; Phone:+49(0)89440074650; Fax:+49(0)89440077534; E-Mail: matthias.brendel@med.uni-muenchen.de

First author:
Christian Sacher (medical student); Department of Nuclear Medicine; LMU Munich, Germany; Phone:+49(0)1623878661; E-Mail: christian.sacher@med.uni-muenchen.de

ABSTRACT

Aim: Non-physiological overexpression of β-amyloid (Aβ) precursor protein in common transgenic Aβ mouse models of Alzheimer's disease (AD) likely hampers their translational potential. The novel *App*$^{NL-G-F}$ mouse incorporates a mutated knock-in, potentially presenting an improved model of AD for Aβ-targeting treatment trials. We aimed to establish serial small animal positron-emission-tomography (μPET) of amyloidosis and neuroinflammation in *App*$^{NL-G-F}$ mice as a tool for therapy monitoring.

Methods: App^{NL-G-F} mice (homozygous n=20; heterozygous n=21) and age-matched wild-type mice (n=12) were investigated longitudinally from 2.5 to 10 months of age with ^{18}F-florbetaben Aβ-μPET and ^{18}F-GE-180 18kDa translocator protein (TSPO)-μPET. Voxel-wise analysis of standardized-uptake-value-ratios (SUVR) images was performed using statistical parametric mapping. All mice underwent a Morris water maze test of spatial learning after their final μPET scan. Quantification of fibrillar Aβ and activated microglia by immunohistochemistry and biochemistry served for validation of μPET results.

Results: The periaqueductal gray emerged as a suitable pseudo-reference tissue for both tracers. Homozygous *App*$^{NL-G-F}$ mice had rising SUVR in cortex and hippocampus for Aβ- (+9.1%, +3.8%) and TSPO- (+19.8%, +14.2%) μPET from 2.5 to 10 months of age (all $p < 0.05$), whereas heterozygous *App*$^{NL-G-F}$ mice did not show significant changes with age. Significant voxel-wise clusters of Aβ deposition and microglial activation in homozygous mice appeared at five months of age. Immunohistochemical and biochemical findings correlated strongly with μPET data. Water maze escape

latency was significantly elevated in homozygous *App*$^{NL-G-F}$ mice compared to wild-type at ten months of age and was associated with high TSPO binding.

Conclusion: Longitudinal µPET in *App*$^{NL-G-F}$ knock-in mice enables monitoring of amyloidogenesis and neuroinflammation in homozygous mice, but is insensitive to minor changes in heterozygous animals. The combination of µPET with behavioral tasks in *App*$^{NL-G-F}$ treatment trails is poised to provide important insights in preclinical drug development.

INTRODUCTION

Alzheimer's disease (AD) is the most common neurodegenerative disease, with an incidence that increases exponentially with age, such that the prevalence exceeds 10% among octagenarians and 30% for nonagenerians. This epidemic is placing a growing socioeconomic burden on health care in societies with aging populations (*1*). The neuropathology of AD classically includes the accumulation of amyloid-β peptide (Aβ) as extracellular plaques, and fibrillary tau aggregates within neurons. Activation of multiple neuroinflammatory pathways mediated by activated microglia expressing high levels of the marker 18-kDa translocator protein (TSPO) completes the triad of markers. These pathologies, mainly restricted to the cerebral cortex and the hippocampus, lead to a progressive decline in cognitive function, usually first manifesting with memory complaints (*2-6*). The identification of familial AD mutations in the amyloid precursor protein (APP) gene has led to the generation of a number of transgenic mouse models that overexpress APP (*7,8*). These first-generation mouse models exhibit AD pathology, but the non-physiological overexpression of APP may cause additional phenotypes unrelated to AD. To circumvent these intrinsic drawbacks, second-generation APP knock-in mice that carry pathogenic mutations in the APP gene have been established (*9*). For example, *App*$^{NL\text{-}G\text{-}F}$ mice carry a mutant APP gene encoding the humanized Aβ sequence (G601R, F606Y, and R609H) with three pathogenic mutations, namely Swedish (KM595/596NL), Beyreuther/Iberian (I641F), and Arctic (E618G). Homozygotic *App*$^{NL\text{-}G\text{-}F}$ mice progressively exhibit widespread Aβ accumulation along with activation of microglia and astrocytes from two months of age, and express behavioral

symptoms in the form of declining spatial learning ability from eight to 12 months of age (*10-13*). Given their physiological expression of APP in comparison to transgenic mouse models, these knock-in mice are not characterized by massively elevated expression of the intracellular domain of APP or soluble APPα (*9*). Therefore, this mouse model potentially avoids confounds due to non-physiological signaling in therapy testing trials.

Previous studies have shown that small animal positron-emission tomography (μPET) is a suitable non-invasive tool for monitoring of therapeutic trials targeting AD pathology (*14,15*). We previously established μPET for monitoring of Aβ deposition and microglial activation in APP-overexpressing mice, yielding excellent correlations with histological and biochemical assessments (*16*). Given this background, the aim of this study was to transfer μPET methodology to the *App*$^{NL-G-F}$ mouse model in a longitudinal investigation of the amyloid tracer ^{18}F-florbetaben (^{18}F-FBB) and the TSPO tracer ^{18}F-GE-180. We confirmed the new dual tracer μPET results relative to findings obtained by immunohistochemistry and biochemistry and correlated the neuropathology findings with scores in a test of spatial learning.

MATERIALS AND METHODS

Animals and Study Design

All experiments were performed in compliance with the National Guidelines for Animal Protection, Germany with the approval of the regional animal committee (Regierung Oberbayern) and were overseen by a veterinarian. Animals were housed in a temperature- and humidity-controlled environment with 12 h light-dark cycle, with free access to food (Sniff, Soest, Germany) and water. The experiments were carried out in mixed sex groups of

heterozygous (n=21) and homozygous (n=20) *App*$^{NL-G-F}$ mice, which is a knock-in mouse line generated by Saito and colleagues (*11*), and a group of age-matched wild-type mice. μPET examinations (Aβ and TSPO) were performed in a longitudinal design at baseline (2.5 months of age) and three follow-up measurements (5.0, 7.5 and 10.0 months). Serial μPET scans of both tracers deriving from a total of 12 age- and sex-matched wild-type mice served as controls, in consideration of the age-dependent increase of cortical TSPO-μPET signal in wild-type mice (*17*). All available mice underwent Morris water maze tests within two weeks after their final μPET scan. After behavioral testing, mice were deeply anaesthetized prior to transcardial perfusion and brain extraction. A minimum number of four brains per genotype were processed for immunohistochemistry and biochemistry in randomly selected hemispheres.

μPET Imaging

μPET Data Acquisition, Reconstruction and Post-Processing: For all μPET procedures, we used an established standardized protocol for radiochemistry, acquisition and pre-processing (*16*). In brief, ^{18}F-GE-180 TSPO-μPET (13.4±1.6 MBq; ~400-1400 GBq/μmol) recordings with an emission window of 60-90 min p.i. were obtained to measure cerebral TSPO expression, along with ^{18}F-FBB Aβ-μPET (12.9±1.7 MBq; ~30-80 GBq/μmol) recordings with an emission window of 30-60 min p.i. for assessment of fibrillar cerebral amyloidosis. Two *App*$^{NL-G-F}$ mice aged eleven months were imaged in a dynamic setting (^{18}F-FBB: 0-60 min p.i.; ^{18}F-GE-180: 0-90 min p.i.) and their results compared to historic dynamic wild-type data for validation of the

previously established time windows in this model. Anesthesia was maintained from just prior to tracer injection to the end of the imaging time window.

μPET Image Analysis: We performed all analyses using PMOD (V3.5, PMOD technologies, Basel, Switzerland). First, intensity normalization of images to standardized-uptake-value (SUV) images was conducted by the previously validated myocardium correction method (*18*) for TSPO-μPET (SUV_{MC}) and by conventional SUV calculation for Aβ-μPET. Voxel-based comparisons of SUV images between $App^{NL\text{-}G\text{-}F}$ (n=13 per tracer, 10 months) and wild-type mice (n=6 per tracer, ten months) were performed to investigate a suitable pseudo-reference tissue for μPET quantification in the $App^{NL\text{-}G\text{-}F}$ mouse model. The judgment of suitability was also informed by the immunohistochemistry results described below. A suitable pseudo-reference tissue was defined as a brain region lacking any genotypic difference in μPET and immunohistochemistry results for both radioligands. These criteria lead us to select the mesencephalic periaqueductal gray (PAG, comprising 20 mm^3) as pseudo-reference region for calculation of SUV-ratio (SUVR) values for both Aβ-μPET and TSPO-μPET (Fig. 1). Two bilateral frontal cortical (CTX) target volumes-of-interest (VOIs, comprising 24 mm^3 each) and two bilateral hippocampal (HIP) target VOIs (comprising 10 mm^3 each) were used for both tracers. Target-to-reference tissue SUVRs were calculated for cortex ($SUVR_{CTX/PAG}$) and hippocampus ($SUVR_{HIP/PAG}$) for Aβ- and TSPO-μPET.

SPM Analysis: For both tracers, whole-brain voxel-wise comparisons of PAG-scaled SUVR images between groups of knock-in and wild-type mice were performed as described previously (*19, 20*).

Behavioral Testing

Mice (homozygous *App*$^{NL-G-F}$: n=11, heterozygous *App*$^{NL-G-F}$: n=14, wild-type: n=3) underwent a Morris water maze test for spatial learning and memory deficits, which was performed according to a standard protocol with small adjustments (*21*). The video tracking software EthoVision® XT (Noldus) was used for analyses of escape latency during the training period as well as at the probe trial.

Immunohistochemistry and Biochemistry

In brain regions corresponding to µPET VOIs (for details see also Supplemental Table 1), histochemistry was performed for fibrillar Aβ (methoxy-X04, TOCRIS) and immunohistochemistry for activated microglia using an Iba1 primary antibody (Wako) as previously established (*17,22*). NAB228 (Santa Cruz) was used for immunohistochemistry labelling of fibrillar as well as non-fibrillar Aβ depositions. Hemispheres from five homozygous *App*$^{NL-G-F}$, five heterozygous *App*$^{NL-G-F}$ and four wild-type mice were used for immunohistochemistry. Assessment of Aβ40 and Aβ42 was performed as previously described (*23*). Biochemical analyses were performed in samples from the entire forebrain. Soluble Trem2 protein was extracted from brain tissue with Tris-buffered saline, and measured by ELISA, using polyclonal sheep antibody for coating (AF1729, R&D Systems) and biotinylated polyclonal sheep antibody (BAF1729, R&D Systems) together with streptavidin-horseradish peroxidase (N-100 ThermoFisher Scientific) for detection. Hemispheres from eight homozygous *App*$^{NL-G-F}$, 14 heterozygous

App^{NL-G-F} and four wild-type were used for biochemical analyses.

Statistics

Group comparisons of VOI-based µPET results between knock-in and wild-type mice were performed by one-way ANOVA and Tukey *post hoc* test for multiple comparisons, calculated by IBM SPSS 25 Statistics (IBM Deutschland GmbH, Ehningen, Germany). Two-sided t-tests were used to compare terminal multimodal readouts of homozygous *App*$^{NL-G-F}$ with wild-type or heterozygous *App*$^{NL-G-F}$ groups. Two-way ANOVA was applied to assess methoxy-X04 and NAB228 fluorescence intensity changes distant and close to plaques. For correlation analyses in *App*$^{NL-G-F}$, Pearson's coefficients of correlation (R) were calculated for normally distributed readouts after Kolmogorov-Smirnov testing for normalcy. For non-normally distributed readouts, Spearman's coefficients of correlation (r_S) were calculated. A threshold of $p<0.05$ was considered significant for rejection of the null hypothesis. Sample size calculations for potential upcoming treatment trials were performed for longitudinal (2.5 to 10.0 months) and terminal measures in the cortical VOI for both ligands in homozygous *App*$^{NL-G-F}$ mice. We used a simplified *t*-statistic model with assumptions of a type I error $\alpha=0.05$, a power of 0.8 and a treatment effect of 50% calculated in G*Power (V3.1, Heinrich-Heine University, Duesseldorf, Germany). For the power calculation we simulated the treatment group by calculating longitudinal differences within single *App*$^{NL-G-F}$ mice and terminal differences of single *App*$^{NL-G-F}$ by multiplying the mean endpoint of wild-type for each tracer by 0.5, corresponding to the 50% treatment effect.

RESULTS

Pseudo Reference Region

Immunohistochemistry revealed a widespread amyloidosis and microglial activation in *App*$^{NL-G-F}$ mice at ten months of age, involving most regions of the forebrain (Fig. 1). Regions with relatively low amyloidosis and microglial activation were observed in parts of the hindbrain, i.e. vermis, midbrain, and notably the PAG. SUV differences between genotypes at ten months of age fitted to immunohistochemistry and revealed lowest ^{18}F-FBB and ^{18}F-GE180 alterations in the hindbrain (Fig. 1). SUV analysis at the final time point revealed that an oval shaped VOI primarily composed of PAG voxels yields a suitable pseudo-reference region (^{18}F-FBB SUV: *App*$^{NL-G-F}$: 0.47 ± 0.08, wild-type: 0.46 ± 0.09, n.s. / ^{18}F-GE180 SUV_{MC}: *App*$^{NL-G-F}$: 0.22 ± 0.02, wild-type: 0.23 ± 0.02, n.s.). $SUVR_{CTX/PAG}$ time-activity-curves of aged *App*$^{NL-G-F}$ mice revealed stable uptake differences for 30-60 min p.i. ^{18}F-FBB and 60-90 min p.i ^{18}F-GE180 imaging when compared to historic wild-type data (Supplemental Fig. 1). Furthermore, the comparison of methoxy-X04 and NAB228 staining revealed only a minor fraction of fibrillar Aβ in amyloid plaques in the entire brain (Fig. 2), which predicted a relatively lower ^{18}F-FBB signal when compared to historically investigated amyloid mouse models.

Dual Tracer µPET Analyses

A comprehensive overview of µPET results is provided in Table 1. The age dependence of the retention of the two tracers is presented in Fig. 3 and illustrated in Supplemental Fig. 2. The voxel-based approach is presented and

discussed in the Supplement including Supplemental Fig. 3.

Aβ-μPET Findings: homozygous *App*$^{NL-G-F}$ mice already showed elevated cortical ^{18}F-FBB SUVR compared to their baseline as early as five months of age (+3.4%; $p<0.05$), which had increased further at ten months (+9.1%; $p<0.001$). Hippocampal increases of SUVR first became apparent at 7.5 months (+2.6%; $p<0.05$) and were more conspicuous at ten months (+3.8%; $p<0.001$). Required sample sizes for detection of a 50% Aβ-μPET treatment effect in the cortex of homozygous *App*$^{NL-G-F}$ mice were n=11 for evaluation of longitudinal measures between 2.5 and 10 months and n=8 for the terminal time-point. The heterozygous genotype did not show significant changes in ^{18}F-FBB SUVR relative to baseline at any age.

TSPO-μPET Findings: homozygous *App*$^{NL-G-F}$ mice revealed the first evidence of increased cortical ^{18}F-GE-180 uptake compared to baseline as early as five months (+6.5%; $p<0.05$), which increased strongly by ten months (+19.8%; $p<0.001$). Significantly elevated ^{18}F-GE-180 SUVR in the hippocampus was present at 7.5 months (+10.8%; $p<0.001$), which increased further by ten months (+14.2%; $p<0.001$). Required sample sizes for detection of a 50% TSPO-μPET treatment effect in the cortex of homozygous *App*$^{NL-G-F}$ mice were n=16 for evaluation of longitudinal measures between 2.5 and 10 months and n=11 for the terminal time-point. The heterozygous genotype revealed neither cortical nor hippocampal microglial activation at any age.

*Correlation Analyses: S*ignificant positive associations between Aβ and TSPO-μPET quantification were observed for the cortex ($R=0.64$; $p<0.001$; Fig. 3C) and the hippocampus ($R=0.48$; $p<0.05$; Fig. 3F).

Correlation with Multimodal Terminal Readouts

Average values for the different genotypes of all terminal readouts at the age of ten months are presented in Supplemental Table 1. We observed strong increases in all biochemical (Aβ40, Aβ42, sTrem2) and (immuno)histochemistry (Iba1, methoxy-X04; see Supplemental Fig. 4) readouts in the comparison of homozygous *App*$^{NL-G-F}$ with wild-type or heterozygous *App*$^{NL-G-F}$ animals. Spatial learning score was substantially impaired in the homozygous *App*$^{NL-G-F}$ compared to wild-type groups (latency to platform +2.1-fold, $p<0.05$, two-tailed), with no such difference for heterozygous *App*$^{NL-G-F}$. All correlations between SUVRs at ten months of age and multimodal terminal readouts are illustrated in Fig. 4.

Biochemistry: Aβ42 concentration correlated highly with cortical ^{18}F-FBB ($r_S=0.69$; $p<0.001$) and ^{18}F-GE-180 uptake ($r_S=0.70$; $p<0.001$). Furthermore, significant Aβ42 correlations with hippocampal SUVRs were observed for both tracers ($p<0.01$). Quantification of sTrem2 correlated with cortical ($r_S=0.61$; $p<0.01$) and hippocampal ($r_S=0.53$; $p<0.05$) SUVR of ^{18}F-GE-180.

Immunohistochemistry: Hippocampal ($r_S=0.90$; $p<0.001$) and cortical ($R=0.75$; $p<0.05$) ^{18}F-FBB uptake was strongly correlated with plaque burden, measured by methoxy-X04 histology in the corresponding regions. The Iba1 burden, which is indicative of activated microglia, correlated with uptake of the TSPO tracer ^{18}F-GE-180 in neocortex ($R=0.92$; $p<0.001$) and hippocampus ($R=0.78$; $p<0.01$).

Behavioral Analysis: There was a moderate significant association between cortical ^{18}F-GE-180 SUVR and escape latency at ten months ($R=0.41$; $p<0.05$), meaning that mice with stronger microglial activation needed

significantly more time to reach the platform in the Morris water maze test.

DISCUSSION

This is the first longitudinal dual-tracer μPET study of cerebral amyloidosis and neuroinflammation in a knock-in AD mouse model. After modification of standardized μPET protocols to circumvent model-specific difficulties in homozygous *App*$^{NL-G-F}$ knock-in mice, we detected strong progressive increases of ^{18}F-FBB and ^{18}F-GE-180 uptake with age. Terminal validation analyses by immunohistochemistry and biochemistry confirmed these *in vivo* μPET results. The present findings establish the basis for serial μPET monitoring of therapeutic agents targeting Aβ deposition and microglial activation in *App*$^{NL-G-F}$ mice.

Two model-specific issues were encountered and solved for establishing μPET imaging in *App*$^{NL-G-F}$ mice: First, the widespread amyloid pathology in brain hampered the use of previously established reference regions such as the cerebellum or white matter (*16*). SUVR scaling by an appropriate intracerebral reference tissue represents an important tool to generate robust μPET results during short acquisition times in mice. This is crucial for the present *App*$^{NL-G-F}$ model mice, which are vulnerable to more stress-related drop-outs compared to other amyloid mouse models (*10*). While full kinetic modelling with arterial blood sampling represents the gold standard for μPET quantification, that approach is hardly feasible in mouse studies encompassing up to four pairs of μPET sessions. Therefore, we made use of a variance analysis for both μPET tracers together with immunohistochemistry assessment to identify the most valid pseudo-reference tissue, which proved

to be PAG of the mesencephalon. Validation in serial dual μPET imaging revealed robust quantification of SUVR relative to PAG, and terminal assessments substantiated our use of this pseudo-reference tissue through the excellent correlation of terminal μPET results with immunohistochemistry gold standards. A low dropout rate during serial μPET imaging (<10% per time-point) also encourage the use of our newly established SUVR protocol. We note that the range SUVR fell below unity for quantification of both tracers, due to higher unspecific binding in the PAG reference tissue when compared to cortical or hippocampal target regions. Using the reference tissue normalization, but reducing variance in the population, stabilized PET quantification, just as in our previous investigations of both ligands (*16,24*).

Another aspect of the present model concerns the fraction of dense fibrillar Aβ in the plaques of *App*$^{NL\text{-}G\text{-}F}$ mice, which is lower than in other transgenic amyloid mouse models. This is an important technicality, as fluorinated Aβ-μPET tracers such as ^{18}F-FBB have high affinity for dense fibrillary plaques, but exhibit only low binding in diffuse plaques (*25*). As expected from this, we observed a lesser longitudinal increase for ^{18}F-FBB binding when compared to ^{18}F-GE-180 from the plaque onset until the full blown pathology occurring at ten months of age (9.1% vs. 19.8%). In contrast, we had earlier found similar increases of the same two radioligands in APP-SL70 (18.3% vs. 17.6%) (*26*) and PS2APP mice (+19.8% vs. +20.2%) (*16*). Thus, while quantitative β-amyloid imaging to ^{18}F-FBB μPET is feasible in *App*$^{NL\text{-}G\text{-}F}$ mice, the tracer misses at least half of the true plaque burden, which constitutes a weakness of using this particular radioligand in the knock-in mouse model. This property needs to be addressed in future studies of Aβ-

targeting therapies or genetic modifications with differential effects on the expressions of dense and diffuse parts of the plaque (*27*).

Serial µPET analyses and terminal assessments of our study indicated parallel increases of amyloidosis and microglial activation with age in the transgenic knock-in mice. The observed strong correlations between cortical TSPO and Aβ readouts were expected from results of a published study, which demonstrated a link between amyloidosis and neuroinflammation based on comparative profiling of cortical gene expression in AD patients and in the *App*$^{NL\text{-}G\text{-}F}$ mouse model (*13*). Our recent study of PS2APP mice showed that the concentration of sTrem2, which is expressed by microglia as a mediator of phagocytic clearance of debris (*6*), is highly correlated with TSPO and Aβ µPET signals (*28*). The present biochemical analysis of sTrem2 also showed strong correlations with terminal TSPO-µPET, but not with Aβ-µPET. This may indicate that sTrem2 serves as a valid biomarker for microglial activation in *App*$^{NL\text{-}G\text{-}F}$ mice, but its expression not so tightly coupled to fibrillar Aβ levels in *App*$^{NL\text{-}G\text{-}F}$ mice when compared to PS2APP mice.

Spatial learning performance at ten months of age (also discussed in the Supplement) did not correlate with longitudinal Aβ-µPET, nor with terminal immunohistochemistry or biochemical measures of amyloidosis, which is in line with a recent review of different transgenic mouse models of AD (*29*). Our previous study with TSPO-µPET in PS2APP revealed some evidence for an association between consistently strong early and terminal neuroinflammation with a better preservation of cognitive function (*30*), suggesting a net protective effect of microglial activation. In contrast, the deterioration in spatial learning in aged *App*$^{NL\text{-}G\text{-}F}$ mice correlated significantly with increased cortical

TSPO-μPET SUVR at the terminal time point. With regard to the specific plaque composition observed in *App*$^{NL-G-F}$, which has less dense but more diffuse plaques in comparison to first generation amyloid mouse models, present findings call for further examination of the specific role of microglial activation in *App*$^{NL-G-F}$ neuropathology. Furthermore, we should in future consider applying other behavioral assessment in addition to the Morris water maze test of spatial learning. Inter-mouse-model comparisons of findings from imaging in conjunction with other biomarkers are summarized in Supplemental Table 2.

Molecular imaging with μPET uniquely affords longitudinal monitoring of disease-related alterations and interventions in individual animals, and can allow prediction of progression and therapeutic effects from early baseline characteristics (*14,15*). Recent therapeutic studies in transgenic mouse models monitored by PET, for instance using an inhibitor of the β-site amyloid precursor protein-cleaving enzyme 1 (BACE1), have already shown encouraging results with respect to delayed pathology (*14,31,32*). Our serial *in vivo* μPET results together with *ex vivo* observations in *App*$^{NL-G-F}$ mice, representing an aggressively neurotoxic knock-in amyloid model with cognitive impairment, support the use of these methods for interventional studies, especially when fibrillary parts of the plaque are targeted by the therapy, as is especially relevant for anti-amyloid antibodies.

CONCLUSION

Analysis of Aβ- and TSPO-μPET imaging in *App*$^{NL-G-F}$ mice is complicated by the widespread cerebral pathology and relatively low fibrillarity

of Aβ plaques, but is feasible using PAG as a pseudo-reference region. Progression of neuropathology can be tracked by serial ^{18}F-FBB and ^{18}F-GE-180 µPET in homozygous *App*$^{NL-G-F}$ mice, whereas heterozygous *App*$^{NL-G-F}$ animals present only minor changes to these methods. The combination of µPET with a test of cognition in this new knock-in AD model *App*$^{NL-G-F}$ is a promising test-bed for preclinical drug development.

Acknowledgements

We thank Karin Bormann-Giglmaier for excellent technical assistance. Florbetaben precursor was provided by Life Molecular. GE made GE-180 cassettes available through an early access model. We acknowledge Inglewood Biomedical Editing for manuscript editing. Seed funding was provided by Verein zur Förderung von Wissenschaft und Forschung an der Medizinischen Fakultät der Ludwig-Maximilians-Universität München. This work was supported by the Deutsche Forschungsgemeinschaft (DFG) by a grant to M.B.&A.R. (BR4580/1-1&RO5194/1-1) and within the framework of the Munich Cluster for Systems Neurology (EXC1010SyNergy).

Conflict of Interest

PB&AR received speaking honoraria from Life Molecular, IB&UN are employees of Novartis. All other authors report no conflicts

KEY POINTS

QUESTION: Is it possible to monitor preclinical trials using amyloid precursor protein (APP) knock-in mice by means of small animal positron-emission-tomography (PET) for β-amyloid and 18kDa translocator protein?

PERTINENT FINDINGS: This longitudinal preclinical investigation revealed progressively increasing uptake of PET tracers for β-amyloid and 18kDa translocator protein in APP knock-in mice. Terminal PET findings were highly correlated with ex vivo gold standard assessments.

TRANSLATIONAL IMPLICATIONS: PET in APP knock-in mice present a new instrument for bench to bedside therapy monitoring without interference from APP overexpression.

References

1. Ziegler-Graham K, Brookmeyer R, Johnson E, Arrighi HM. Worldwide variation in the doubling time of Alzheimer's disease incidence rates. *Alzheimers Dement.* 2008;4:316-323.

2. Braak H, Braak E. Demonstration of amyloid deposits and neurofibrillary changes in whole brain sections. *Brain Pathol.* 1991;1:213-216.

3. Hyman BT, Phelps CH, Beach TG, et al. National Institute on Aging-Alzheimer's Association guidelines for the neuropathologic assessment of Alzheimer's disease. *Alzheimers Dement.* 2012;8:1-13.

4. Serrano-Pozo A, Frosch MP, Masliah E, Hyman BT. Neuropathological alterations in Alzheimer disease. *Cold Spring Harb Perspect Med.* 2011;1:a006189.

5. Querfurth HW, LaFerla FM. Alzheimer's disease. *N Engl J Med.* 2010;362:329-344.

6. Heneka MT, Carson MJ, Khoury JE, et al. Neuroinflammation in Alzheimer's disease. *Lancet Neurol.* 2015;14:388-405.

7. Jonsson T, Atwal JK, Steinberg S, et al. A mutation in APP protects against Alzheimer's disease and age-related cognitive decline. *Nature.* 2012;488:96-99.

8. Hsiao K, Chapman P, Nilsen S, et al. Correlative memory deficits, Abeta elevation, and amyloid plaques in transgenic mice. *Science.* 1996;274:99-102.

9. Sasaguri H, Nilsson P, Hashimoto S, et al. APP mouse models for Alzheimer's disease preclinical studies. *EMBO J.* 2017;36:2473-2487.

10. Masuda A, Kobayashi Y, Kogo N, Saito T, Saido TC, Itohara S. Cognitive deficits in single App knock-in mouse models. *Neurobiol Learn Mem.* 2016;135:73-82.

11. Saito T, Matsuba Y, Mihira N, et al. Single App knock-in mouse models of Alzheimer's disease. *Nat Neurosci.* 2014;17:661-663.

12. Sakakibara Y, Sekiya M, Saito T, Saido TC, Iijima KM. Cognitive and emotional alterations in App knock-in mouse models of Abeta amyloidosis. *BMC Neurosci.* 2018;19:46.

13. Castillo E, Leon J, Mazzei G, et al. Comparative profiling of cortical gene expression in Alzheimer's disease patients and mouse models demonstrates a link between amyloidosis and neuroinflammation. *Sci Rep.* 2017;7:17762.

14. Brendel M, Jaworska A, Overhoff F, et al. Efficacy of chronic BACE1 inhibition in PS2APP mice depends on the regional Abeta deposition rate and plaque burden at treatment initiation. *Theranostics.* 2018;8:4957-4968.

15. Brendel M, Jaworska A, Herms J, et al. Amyloid-PET predicts inhibition of de novo plaque formation upon chronic γ-secretase modulator treatment. *Mol Psychiatry.* 2015;20:1179-1187.

16. Brendel M, Probst F, Jaworska A, et al. Glial activation and glucose metabolism in a transgenic amyloid mouse model: A triple-tracer PET Study. *J Nucl Med.* 2016;57:954-960.

17. Brendel M, Focke C, Blume T, et al. Time courses of cortical glucose metabolism and microglial activity across the life span of wild-type mice: A PET study. *J Nucl Med.* 2017;58:1984-1990.

18. Deussing M, Blume T, Vomacka L, et al. Coupling between physiological TSPO expression in brain and myocardium allows stabilization of late-phase cerebral [(18)F]GE180 PET quantification. *Neuroimage.* 2018;165:83-91.

19. Rominger A, Brendel M, Burgold S, et al. Longitudinal assessment of cerebral b-amyloid deposition in mice overexpressing Swedish mutant b-amyloid precursor protein using 18F-florbetaben PET. *J Nucl Med.* 2013;54:1127-1134.

20. Sawiak SJ, Wood NI, Williams GB, Morton AJ, Carpenter TA. Voxel-based morphometry in the R6/2 transgenic mouse reveals differences between genotypes not seen with manual 2D morphometry. *Neurobiol Dis.* 2009;33:20-27.

21. Bromley-Brits K, Deng Y, Song W. Morris water maze test for learning and memory deficits in Alzheimer's disease model mice. *J Vis Exp.* 2011. 2011;53:e2920

22. Dorostkar MM, Dreosti E, Odermatt B, Lagnado L. Computational processing of optical measurements of neuronal and synaptic activity in networks. *J Neurosci Methods.* 2010;188:141-150.

23. Neumann U, Rueeger H, Machauer R, et al. A novel BACE inhibitor NB-360 shows a superior pharmacological profile and robust reduction of amyloid-beta and neuroinflammation in APP transgenic mice. *Mol Neurodegener.* 2015;10:44.

24. Overhoff F, Brendel M, Jaworska A, et al. Automated spatial brain normalization and hindbrain white matter reference tissue give improved [18F]-florbetaben PET quantitation in Alzheimer's model mice. *Front Neurosci.* 2016;10:45.

25. Catafau AM, Bullich S, Seibyl JP, et al. Cerebellar amyloid-beta plaques: How frequent are they, and do they influence 18F-Florbetaben SUV ratios? *J Nucl Med.* 2016;57:1740-1745.

26. Blume T, Focke C, Peters F, et al. Microglial response to increasing amyloid load saturates with aging: a longitudinal dual tracer in vivo muPET-study. *J Neuroinflammation.* 2018;15:307.

27. Ulrich JD, Ulland TK, Mahan TE, et al. ApoE facilitates the microglial response to amyloid plaque pathology. *J Exp Med.* 2018;215:1047-1058.

28. Brendel M, Kleinberger G, Probst F, et al. Increase of TREM2 during aging of an Alzheimer's disease mouse model Is paralleled by microglial activation and amyloidosis. *Front Aging Neurosci.* 2017;9:8.

29. Foley AM, Ammar ZM, Lee RH, Mitchell CS. Systematic review of the relationship between amyloid-beta levels and measures of transgenic mouse cognitive deficit in Alzheimer's disease. *J Alzheimers Dis.* 2015;44:787-795.

30. Focke C, Blume T, Zott B, et al. Early and longitudinal microglial activation but not amyloid accumulation predict cognitive outcome in PS2APP mice. *J Nucl Med.* 2019;60:548-554.

31. Deleye S, Waldron AM, Verhaeghe J, et al. Evaluation of small-animal PET outcome measures to detect disease modification induced by BACE

inhibition in a transgenic mouse model of Alzheimer disease. *J Nucl Med.* 2017;58:1977-1983.

32. Meier SR, Syvanen S, Hultqvist G, et al. Antibody-based in vivo PET imaging detects amyloid-beta reduction in alzheimer transgenic mice after BACE-1 inhibition. *J Nucl Med.* 2018;59:1885-1891.

Tables and Figures

Table 1: Overview of µPET results

Group	Age			Amyloid-µPET				TSPO-µPET	
	months	n	sex	Cortex (SUVR)	Hippocampus (SUVR)	n	sex	Cortex (SUVR)	Hippocampus (SUVR)
App^{NL-G-F}	2.5	20	9♂/11♀	0.86±0.02	0.95±0.01	18	9♂/9♀	0.79±0.05	0.82±0.04
(homozygous)	5.0	17	6♂/11♀	0.89±0.03*	0.96±0.02	17	6♂/11♀	0.84±0.04*	0.86±0.03
	7.5	13	6♂/7♀	0.92±0.05***	0.97±0.03*	14	6♂/8♀	0.91±0.04***	0.91±0.06***
	10	13	6♂/7♀	0.94±0.03***	0.98±0.02***	13	6♂/7♀	0.94±0.06***	0.94±0.07***
App^{NL-G-F}	2.5	21	13♂/8♀	0.87±0.03	0.95±0.03	20	12♂/8♀	0.78±0.06	0.81±0.04
(heterozygous)	5.0	20	12♂/8♀	0.87±0.04	0.94±0.02	20	12♂/8♀	0.78±0.05	0.81±0.04
	7.5	15	9♂/6♀	0.89±0.04	0.95±0.02	17	10♂/7♀	0.77±0.04	0.81±0.05
	10	13	8♂/5♀	0.89±0.04	0.95±0.03	13	8♂/5♀	0.79±0.04	0.81±0.05
C57BL/6	2.5	6	3♂/3♀	0.87±0.03	0.96±0.01	6	3♂/3♀	0.75±0.07	0.80±0.04
(wild-type)	10	6	3♂/3♀	0.86±0.01	0.95±0.01	6	3♂/3♀	0.82±0.04	0.84±0.03

P-values for one-way ANOVA including *post-hoc* Tukey testing versus baseline given by: *p<0.05; ***p<0.001. Numbers (n) of mice included in PET analyses by sex are provided for each tracer and age.

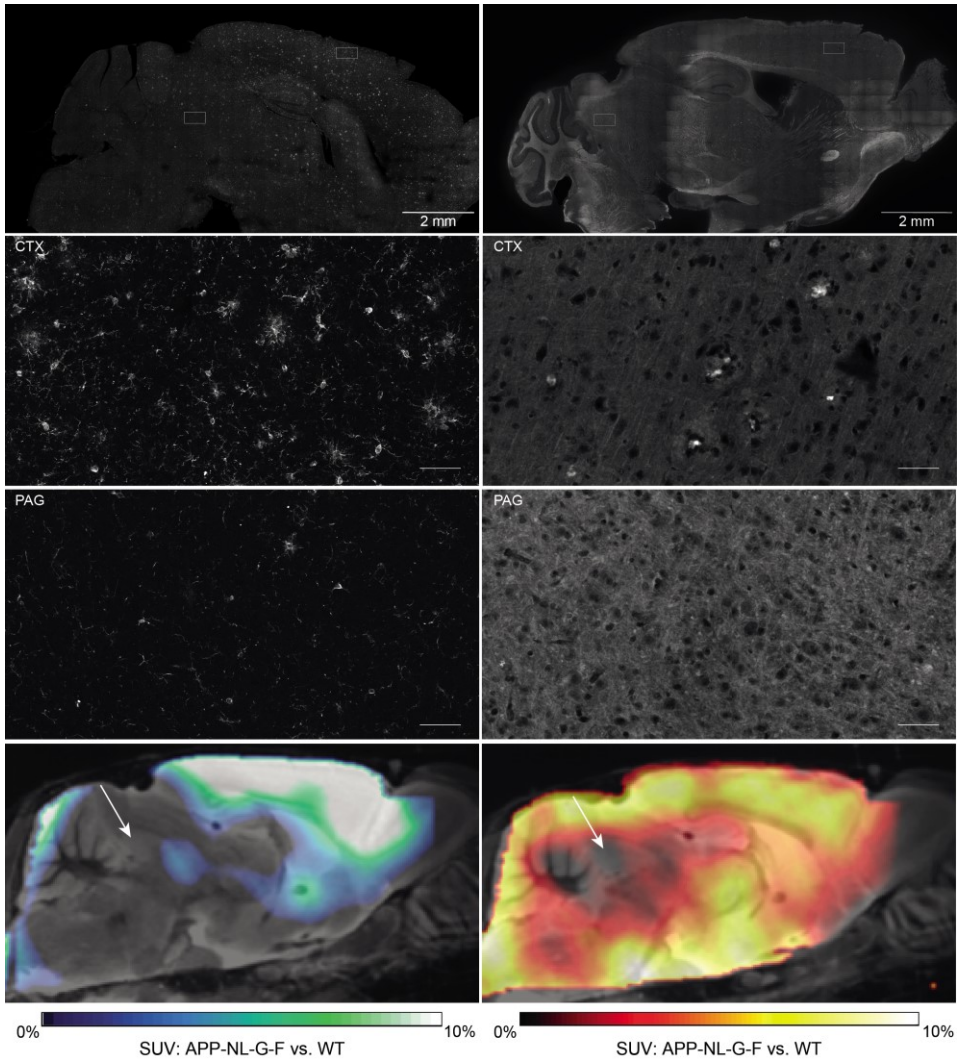

Figure 1: Immunohistochemistry reveals lowest microglia activation (left, Iba-1) and amyloid deposition (right, methoxy-X04) in the periaqueductal gray (PAG) of *App*$^{NL\text{-}G\text{-}F}$ mice aged ten months (overview and zoom in the upper three panels). Suitability of the PAG as a pseudo-reference tissue was further assessed by comparing SUV of TSPO- and Aβ-PET images between genotypes (overview in the lowest panel).

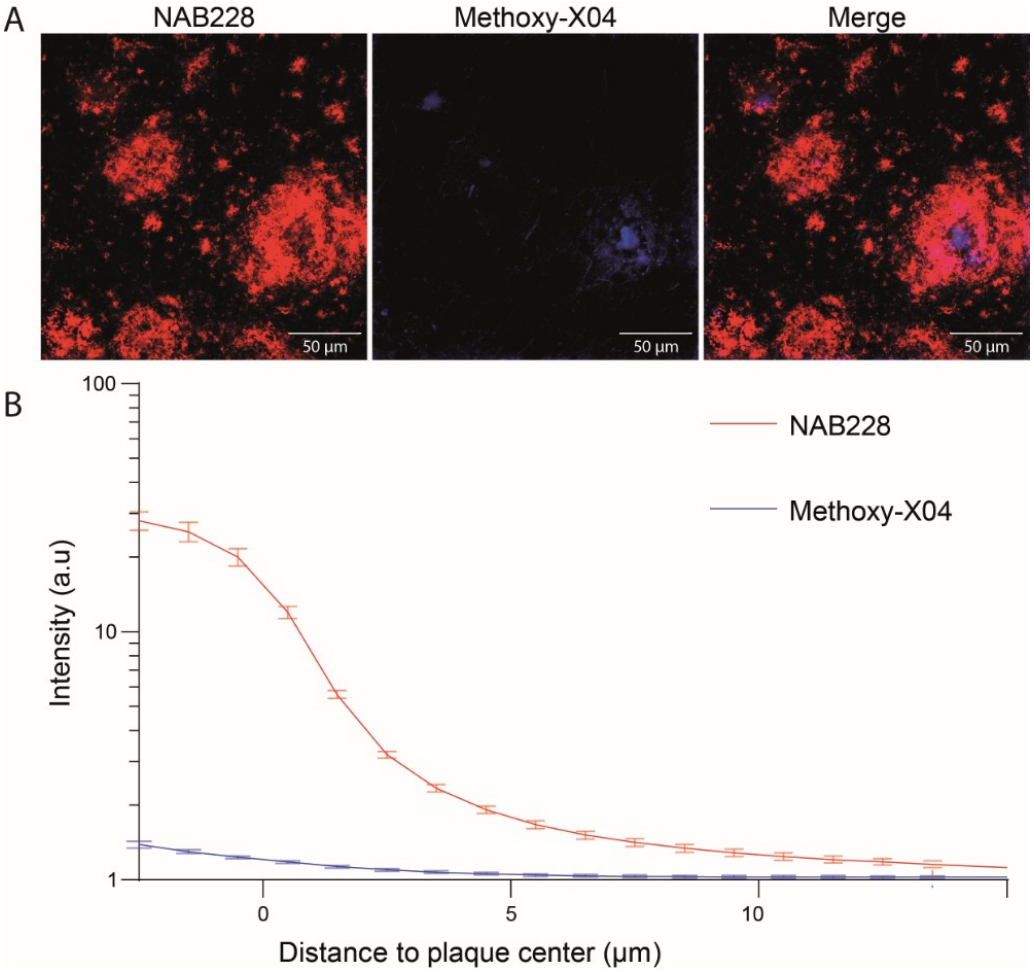

Figure 2: Minor dense fraction of cortical β-amyloid plaques in *App*$^{NL-G-F}$ mice as assessed by NAB228 (red) and methoxy-X04 (blue) co-staining. The graph indicates mean Methoxy-X04 and NAB228 fluorescence intensity profiles from the plaque border; two-way ANOVA interaction staining x distance $F_{(43,704)}$=14.79, p<0.001. Data presented as mean ± SEM with ***p<0.001; n=9 mice per group; minimal plaque number analyzed per mouse: 41.

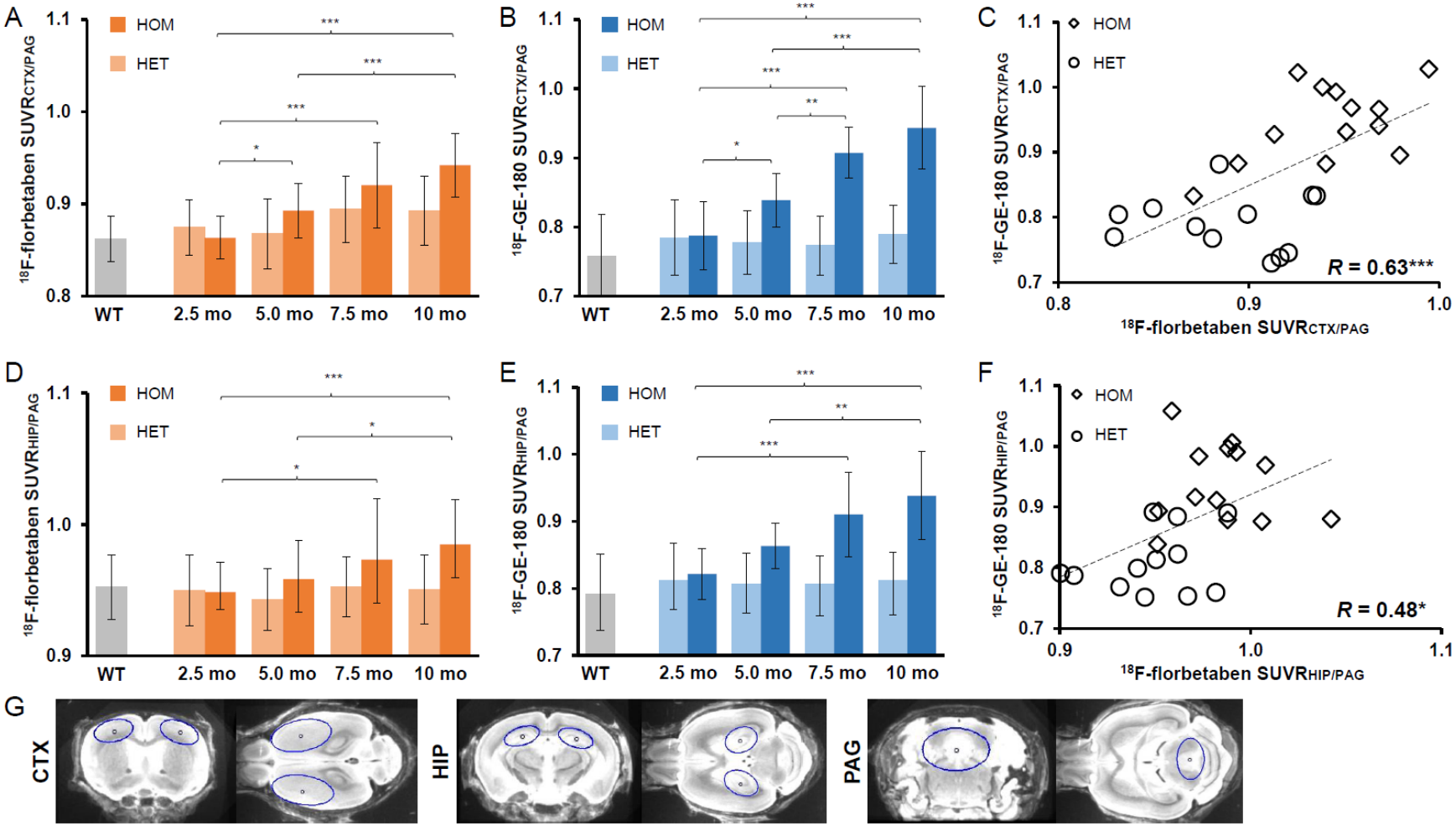

Figure 3: (**A,B,D,E**) Age dependence of Aβ and TSPO radiotracer uptake in in the frontal cortex and in the hippocampus of homozygous (HOM) and heterozygous (HET) *App*$^{NL\text{-}G\text{-}F}$ mice. Group comparisons of VOI-based µPET results between knock-in mouse groups were assessed by one-way ANOVA and Tukey *post hoc* test. (**C,F**) Correlation between Aβ-deposition and microglial activation in the frontal cortex and in the hippocampus measured by dual tracer µPET (R indicate Pearson's coefficients of correlation). *p<0.05; **p<0.01; ***p<0.001. (**G**) Definitions of cortical (CTX), hippocampal (HIP) and periaqueductal gray (PAG) VOIs in coronal and axial slices upon an MRI mouse brain atlas.

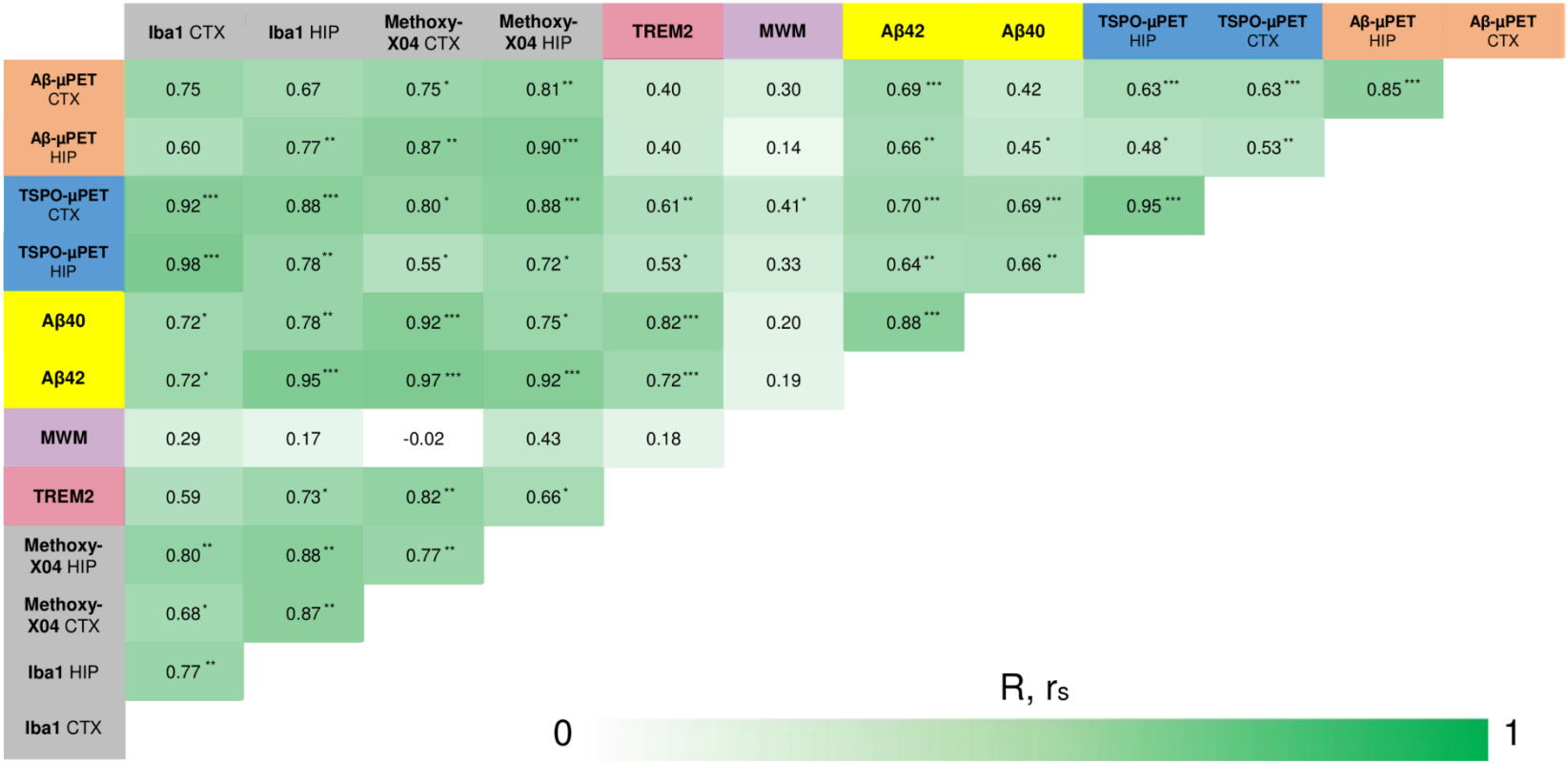

Figure 4: Correlation analyses of all terminal readouts. Pearson's coefficients of correlation (R) were calculated for normally distributed readouts (μPET, behaviour, Iba1, methoxy-X04). For the remaining not normally distributed readouts, Spearman's coefficients of correlation (r_S) were calculated. *p<0.05; **p<0.01; ***p<0.001